Desalination and Water Treatment
www.deswater.com
doi: 10.5004/dwt.2019.24744

170 (2019) 297–307
December

Preparation of Ag_3PO_4/CNH and the performance for photocatalytic degradation of microcystin-LR under visible light

Jun Xu, Shanqing Jiang, Jiahui Ma, Qiuya Zhang, Hui Peng, Li Jiao, Liping Wang*

School of Environmental & Safety Engineering, Changzhou University, Changzhou 213164, China, Tel. +86-13915038128; Fax: +86-0519-86330087; email: wlp@cczu.edu.cn (L.P. Wang), Tel. +86-18352560047; email: 1031949918@qq.com (J. Xu), Tel. +86-15961256380; email: jiangshanqing@cczu.edu.cn (S.Q. Jiang), Tel. +86-0519-86330087; email: 150923420@qq.com (J.H. Ma), Tel. +86-0519-86330087; email: 793544260@qq.com (Q.Y. Zhang), Tel. +86-15851937251; email: 1395237564@qq.com (H. Peng), Tel. +86-0519-86330087; email: 1967851677@qq.com (L. Jiao)

Received 2 April 2019; Accepted 24 July 2019

ABSTRACT

Protonated g-C_3N_4 (CNH) was prepared with g-C_3N_4 powder by HNO_3 hydrothermal method, and Ag_3PO_4/CNH composite was further synthesized by chemical precipitation. The prepared samples were characterized by X-ray diffraction, Fourier transform infrared spectra, UV–Vis diffuse reflectance spectrometer, scanning electron microscopy, energy dispersive X-ray spectroscopy, transmission electron microscopy, photoluminescence spectra and electron spin resonance. The photocatalytic performance of Ag_3PO_4/CNH under visible light was evaluated by the microcystin-LR (MC-LR) degradation experiment. The results showed that Ag_3PO_4 could be successfully loaded on the surface of CNH, and its light absorption intensity was significantly improved compared with CNH. When the mass ratio of Ag_3PO_4 was 20% in Ag_3PO_4/CNH composite, the photodegradation efficiency of MC-LR was the highest under the condition of visible light irradiation for 2 h with the degradation rate of 79.8% which was 5.4 times higher than that of pure CNH and 9.8 times higher than that of pure g-C_3N_4. The photodegradation reaction of Ag_3PO_4/CNH for MC-LR was in line with quasi-first-order kinetic model. The scavenger tests proved that $\cdot O_2^-$ and h^+ played the major role in the degradation process. A possible Z-scheme degradation mechanism of MC-LR over Ag_3PO_4/CNH hybrid was proposed.

Keywords: Ag_3PO_4; Protonated g-C_3N_4; Visible-light photocatalysis; Microcystin-LR; Z-scheme degradation mechanism

1. Introduction

With the development of human society, the discharge of nitrogen and phosphorus-containing wastewater is gradually increasing, and the phenomenon of eutrophication of water is becoming more and more severe [1]. Since 2007, cyanobacteria in the Taihu Lake Basin will explode in large areas in summer, and the water ecology will be seriously damaged and odor will be emitted [2], which will have a major impact on the lives of surrounding residents. At the same time, cyanobacteria also release a variety of algal toxins, among which microcystin (LR type, MC-LR) are most common and toxic, and are highly concerned by researchers [3]. MC-LR is a biologically active monocyclic polypeptide compound whose structure Adda group determines the physiological activity of the toxin and easily causes serious damage to the liver of animals and humans [4]. Common techniques currently used for MC-LR degradation are adsorption [5], biological [6] and ozone oxidation [7]. The adsorption method increases the cost due to frequent replacement of materials, although the biological method is low in cost but the degradation process is too slow [8], the ozonation method can efficiently remove algal toxins but will produce carcinogenic by-products [9]. Recently, it has been found that the Adda group in the MC-LR structure can be destroyed by photocatalysis, and the

* Corresponding author.

photocatalytic technology is highly efficient and stable, without secondary pollution [10]. Therefore, the development of new visible-light catalytic materials for the degradation of MC-LR will be of great significance.

As a new type of visible light-responsive non-metallic material, graphite-like carbon nitride (g-C_3N_4) has been widely used due to its narrow band gap, good chemical stability, excellent electronic, optoelectronic properties and simple preparation method [11–15], it also plays an important role in catalyzing organic synthesis [12], degrading organic pollutants [13], electrochemistry [14], photosplitting of water [16], photoreduction of carbon dioxide [17], etc. However, the g-C_3N_4 has the shortcomings of small specific surface area, weak visible-light response and high electron–hole recombination rate which limits its practical application [13,18]. Therefore, researchers have been exploring new ways to overcome these shortcomings, including the use of template and template-free methods [19], precious metal deposition [20], composite formation of heterojunction [21] and other methods. The template method and the template-free method can improve the specific surface area of g-C_3N_4, but the template method has the disadvantages of high synthesis cost and easy to cause secondary pollution, while the template-free method requires high accuracy for acidity and alkalinity during the experiment, and the preparation process is difficult to repeat [22]. Although precious metal deposition expands the absorption range of light and enhances light absorption, excessive precious metals will become new electron–hole recombination centers, which reduce the catalytic efficiency [20]. In comparison, the method of composite forming a heterojunction has high catalytic efficiency and no secondary pollution [21].

In the existing research, g-C_3N_4 is combined with TiO_2 [23], CdS [24], Bi_2WO_6 [25], AgX (X = Cl, Br, I) [26], MoS_2 [27], Bi_5O_7I [28] and other semiconductors to form a heterojunction to improve its photocatalytic performance [29,30]. At the same time, Ag_3PO_4 has received extensive attention due to its great photocatalytic performance. Yi et al. [31] reported that Ag_3PO_4 has excellent photocatalytic activity for water decomposition and degradation of organic pollutants under visible-light irradiation. However, the disadvantage of easy agglomeration of Ag_3PO_4 particles limits its further development [32]. Based on the reported research, the construction of Ag_3PO_4-based heterostructure photocatalysts with other semiconductors is an efficient way, such as Ag_3PO_4/CdS [33], Ag_3PO_4/TiO_2 [34], Ag_3PO_4/BiOI [35], Ag_3PO_4/ZnO [36], $ZnWO_4/Ag_3PO_4$ [37], $Ag_3PO_4/NiFe_2O_4$ [38]. All of these composites exhibit an enriched separation of charge, structural stability and photocatalytic efficiency. So far, few studies focused on Ag_3PO_4 and g-C_3N_4 photocatalytic elimination of MC-LR in aqueous solutions. It may be a good choice to combine Ag_3PO_4 with protonated g-C_3N_4 to degrade MC-LR.

Considering the excellent photooxidation activity of Ag_3PO_4 and excellent electronic, optoelectronic properties of g-C_3N_4, a heterojunction photocatalyst between g-C_3N_4 and Ag_3PO_4 can be constructed. In this study, g-C_3N_4 prepared by high temperature calcination was used as the substrate, protonated g-C_3N_4 (CNH) nanomaterials was prepared by nitric acid hydrothermal method, and Ag_3PO_4/CNH composite was further synthesized by chemical precipitation. The photocatalytic performance under visible light was investigated by the degradation of MC-LR. Multiple physicochemical techniques were carried out, and the possible mechanism of the photocatalytic activity is also proposed.

2. Experimentation

2.1. Materials

Melamine ($C_3H_6N_6$, 99%), nitric acid (HNO_3, 69%), ethanol (C_2H_5OH, 99.7%, ANHY), trisodium phosphate ($Na_3PO_4{\cdot}12H_2O$, 99%) and silver nitrate ($AgNO_3$, 99%) were purchased from Sinopharm Chemical Reagent Co. Ltd., (Shanghai, China). All of the reagents used above were of analytical grade and not further purified. P-benzoquinone (BQ, 99%), ethylene diamine tetraacetic acid disodium salt (EDTA-2Na, 99%) and tertiary butanol (t-BuOH, 99%) were purchased from Aladdin (Shanghai, China). Methanol (CH_3OH, 99.9%, UV-HPLC-gradient grade) was purchased from ANPEL Laboratory Technologies (Shanghai) Inc. Water used in the experiment was deionized water.

2.2. Culture of Microcystis and extraction of MC-LR

Culture of *Microcystis*: The *Microcystis aeruginosa* was purchased from the Wuhan Institute of Hydrobiology, Chinese Academy of Sciences, and cultured in BG-11 medium at a temperature of 25°C. The lighting conditions were automatic light/dark cycle every 12 h and the illumination was 2,000lx [39].

Extraction of MC-LR: 1,000 mL cultures were sequentially subjected to repeated freezing and heating three times after a 30-d incubation. Then the algae solution was ultrasonically shaken for 1 h by the ultrasonic system, centrifuged at high speed (4,500 rpm, 30 min) and sequentially filtered under reduced pressure through a GF/C glass fiber membrane and a 0.45 μm cellulose acetate filter. Next, the solid-phase extraction device was connected, and the obtained filtrate was injected into the activated C_{18} solid-phase extraction cartridge for enrichment. After the enrichment was completed, the *Microcystis* were eluted with the eluent and collected in a glass container. Finally, the purified MC-LR was obtained by blowing off with nitrogen [3,40].

2.3. Preparation of photocatalytic composites

Preparation of g-C_3N_4: 30 g of melamine was placed in a 100 mL semi-closed alumina crucible and placed in a muffle furnace (SX2-4-13, Shanghai-Hede) for calcination at 550°C for 4 h. The heating rate was controlled at 2.3°C/min. After the reaction, the sample was cooled to constant temperature and ground to obtain a yellow g-C_3N_4 powder.

Preparation of protonated g-C_3N_4 (CNH): 1 g of the prepared g-C_3N_4 powder was added to 40 mL of 0.5 mol/L HNO_3 solution, and the powder was uniformly dispersed by magnetic stirring for 30 min. Then, the suspension was placed in a high-pressure autoclave (Jinan Henghua Technology, China) and reacted at 160°C for 7 h. After cooling, the resulting powder was thoroughly washed with absolute ethanol and deionized water, and dried at 80°C for 10 h in a vacuum drying oven. The final product is labeled as CNH.

Preparation of Ag_3PO_4/CNH composites: 0.1, 0.2 and 0.3 g of $AgNO_3$ were dissolved in 100 mL of deionized water,

respectively, then 1 g of CNH dispersed in the solutions by ultrasonic for 30 min. Afterwards, 100 mL aqueous solutions of $Na_3PO_4{\cdot}12H_2O$ (0.165, 0.33 and 0.495 g) were added dropwise to the $AgNO_3$ and CNH mixture under strong magnetic stirring and maintained for 4 h in the dark. The acquired composites were thoroughly cleaned four times with absolute ethanol and deionized water, then dried at 80°C for 10 h in a vacuum oven. Finally, different Ag_3PO_4/CNH composites with Ag_3PO_4 mass ratios of 10%, 20% and 30% were obtained. They were labeled as Ag_3PO_4/CNH (10 wt.%), Ag_3PO_4/CNH (20 wt.%) and Ag_3PO_4/CNH (30 wt.%), respectively.

2.4. Characterization methods

The crystal phases of g-C_3N_4, CNH and Ag_3PO_4/CNH were analyzed by X-ray diffraction (XRD, Rigaku, Japan) which used step scanning. XRD patterns was performed on a D/max-2500 PC with a high power Cu Kαl radioactive source (λ = 0.15406 nm) at 60 kV/30 mA, and the scanning frequency was 0.04°/0.4 s, scan angle 2θ range was 10°–80°. The morphological characteristics of g-C_3N_4, CNH and Ag_3PO_4/CNH were analyzed by using a scanning electron microscopy (SEM, SUPRA55, Zeiss, Germany), and transmission electron microscopy (TEM) were carried out using JEM-2100 equipment. The composition of the material was explored by energy dispersive X-ray spectroscopy (EDS). The light absorption properties of CNH and Ag_3PO_4/CNH was measured by UV–Vis diffuse reflectance spectrometer (DRS) which was performed on a UV-3600 spectrometer and was using $BaSO_4$ as a reference within scanning range of 200–800 nm. (Shimadzu, Japan) The composition and functional groups of CNH and Ag_3PO_4/CNH were determined by Fourier transform infrared spectra (FT-IR, Nicolet iS50, Thermo fisher, USA) using KBr as a reference. Photoluminescence (PL) spectra were obtained on the fluorescence spectrometer (Cary Eclipse, USA). The active group of the sample was determined by an electron spin resonance (ESR) analyzer (Bruker A300, Germany).

2.5. Photocatalytic degradation of MC-LR experiment

The photocatalytic degradation experiment of MC-LR was carried out in an XPA-system photochemical reactor (Nanjing Xujiang, China) in which the light source is 350-W Xe lamp with a 420 nm cut-off filter. At room temperature, 10 mL of 15 mg L^{-1} MC-LR solution was taken into the quartz glass tube and 0.05 g of the prepared samples (g-C_3N_4, CNH and Ag_3PO_4/CNH) were dispersed into it. For eliminating the influence of adsorption, the suspension was magnetically stirred in the dark for 60 min before irradiation to reach the adsorption-desorption equilibrium. After the dark reaction, the light source was switched on to initiate the photocatalytic degradation reaction. During the reaction, 1 mL of the mixed solution was taken every 30 min and the catalyst particles were removed by centrifugation and microfiltration (0.45 μm), then the concentration of MC-LR in the solution was determined by liquid chromatography [41,42].

The concentration of MC-LR was analyzed by high-performance liquid chromatography (Agilent-1200, Agilent, USA) using a C_{18} column (2.6 μm, 2.1 × 50 mm) with a sample injection volume of 20 μL and the detection wavelength is 230 nm. Each sample was tested three times, and the results were averaged. The specific calculation of MC-LR degradation rate (D) was calculated by Eq. (1):

$$D = \frac{C_0 - C}{C_0} \times 100\% \quad (1)$$

where D (%) is the degradation rate, C_0 (mg L^{-1}) is the initial concentration of MC-LR, and C (mg L^{-1}) is the concentration of MC-LR in the sample taken every 30 min.

3. Results and discussion

3.1. Characterization of photocatalytic materials

3.1.1. XRD analysis

XRD was used to analyze the crystal phases of the monomers g-C_3N_4 and CNH before and after HNO_3 etching. As shown in Fig. 1a, it can be clearly seen from the figure that the monomer g-C_3N_4 and CNH have two characteristic diffraction peaks at positions near 2θ of 13.08° and 27.41°, respectively, corresponding to the main characteristic peaks of the (100) and (002) crystal plane in g-C_3N_4. All the characteristic peaks of the samples can be well indexed to the characteristic peaks of g-C_3N_4 in the card (JCPDS: 087-1526) [43]. It indicated that the phase did not change significantly before and after the HNO_3 etching treatment. However, the (100) crystal plane of CNH had a weaker crystal plane strength compared with g-C_3N_4, indicating that the nitric acid reaction had an effect on the partial structure of g-C_3N_4. Meanwhile the (002) crystal plane of CNH was moved from 27.41° to 27.50°, which indicated that the interlayer spacing of CNH was reduced after hydrothermal acid treatment and improved the interlayer stacking degree of CNH [44].

Fig. 1b further compares the XRD patterns of CNH and three different mass ratios (10 wt.%, 20 wt.% and 30 wt.%) of Ag_3PO_4/CNH composites. It is apparent that in addition to the (100) and (002) characteristic crystal planes of g-C_3N_4, there were also diffraction peaks at 2θ of 20.78°, 29.59°, 33.20°, 36.48°, 42.38°, 47.70°, 52.69°, 54.92°, 57.18°, 60.14°, 65.72°, 69.80°, 71.80° and 73.76°, respectively corresponding to the (110), (200), (210), (211), (220), (310), (222), (320), (321), (400), (330), (420), (421) and (322) crystal plane in Ag_3PO_4. All the diffraction peaks of the samples can be well indexed to the diffraction peaks of Ag_3PO_4 in the standard card (JCPDS: 06-0505) [45]. No obvious peaks of Ag_3PO_4 at 69.80°, 71.80°and 73.76° are detected in Ag_3PO_4/CNH composites when the mass of Ag_3PO_4 is less than 20 wt. %, indicating that Ag_3PO_4 did not enter the CNH lattice and did not cause changes in the internal structure of CNH, but only dispersed and anchored on the surface of CNH. As the Ag_3PO_4 content increased, the peak intensity of CNH decreased. Moreover, no additional diffraction peaks are observed in Ag_3PO_4/CNH composites indicating that Ag_3PO_4 and CNH remain pure and stable. Therefore no by-products were formed during the recombination of Ag_3PO_4 and CNH.

3.1.2. FT-IR analysis

Fig. 2 shows the FT-IR spectra of CNH and three different mass ratios of Ag_3PO_4/CNH. It can be seen from the figure that a characteristic peak belonging to g-C_3N_4 appears

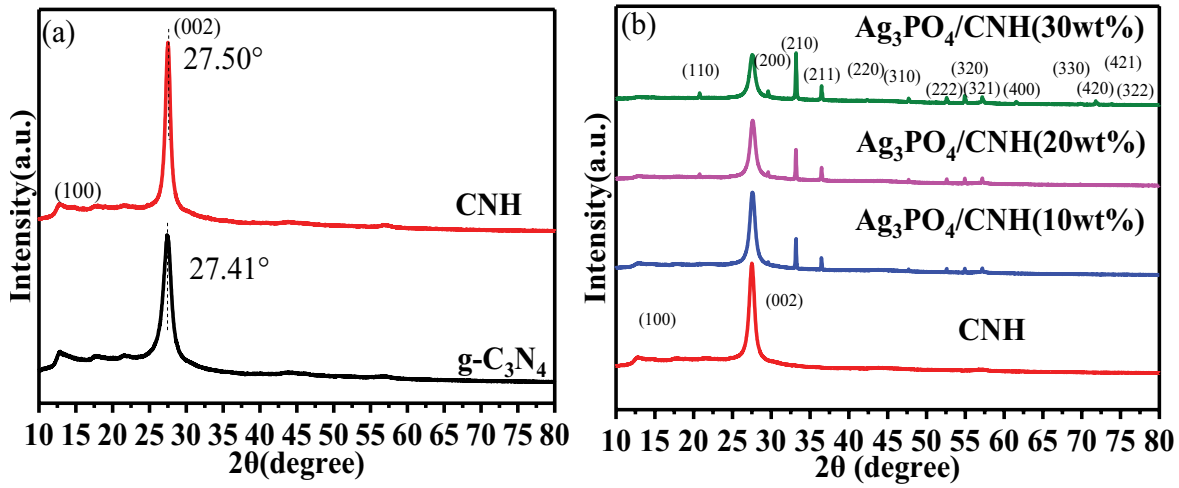

Fig. 1. XRD patterns: (a) g-C_3N_4 and CNH and (b) Ag_3PO_4/CNH.

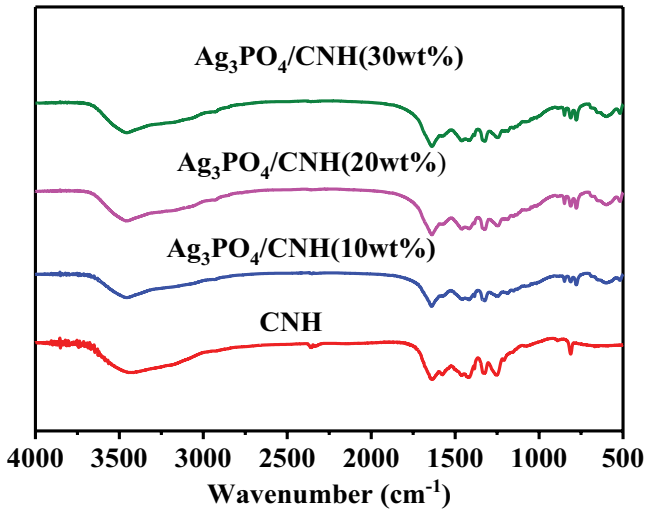

Fig. 2. FT-IR spectra of CNH and Ag_3PO_4/CNH.

on the spectra of CNH [46], wherein the broad peak at 2,800–3,600 cm^{-1} is derived from the stretching vibration of NH_2 at the end of the NH group which is at the aromatic ring defect site. The peak at 1,340–1,465 cm^{-1} is a typical vibration ring. The peaks around 1,255; 1,329 and 1,406 cm^{-1} correspond to C–N stretching vibrations. The peak around 1,635 cm^{-1} is mainly attributed to the stretching vibration of the C=N bond, while the peak around 810 cm^{-1} is the characteristic peak of the triazine ring [47]. Furthermore, the peaks of Ag_3PO_4/CNH composites around 928 and 541 cm^{-1} may be attributed to the characteristic peaks of PO_4^{3-} [34]. The peak at 850 cm^{-1} is assigned to the P–O–P stretching vibrations, while the peak at 560 cm^{-1} is ascribed to the O=P–O bending vibration [48]. Additionally, all the characteristic peaks of CNH are contained in Ag_3PO_4/CNH composites, indicating that Ag_3PO_4 and CNH were successfully compounded together.

3.1.3. DRS analysis

The light absorption properties of the prepared pure CNH and three mass ratios (10, 20 and 30 wt.%) of Ag_3PO_4/CNH composite photocatalytic materials were detected by UV–Vis diffuse reflectance spectrometer, and the results are shown in Fig. 3a. It can be seen that the maximum absorption band edge of the sample doped with Ag_3PO_4 was red-shifted compared with pure CNH, mainly because the absorption ability of the composite to visible light was gradually enhanced as the amount of Ag_3PO_4 doping increased.

In addition, the band gap energy of the semiconductor catalytic material can be calculated by the relationship between $(\alpha hv)^2$ and hv, as shown in Eq. (2).

$$\alpha hv = A(hv - E_g)^{n/2} \quad (2)$$

where α, h, v, A and E_g represent the absorption coefficient, Planck constant, emission light frequency, constant and photonic energy band gap, respectively. n = 1 or 4 (the direct conductor is n = 1 and the indirect conductor is n = 4). According to Eq. (2), the band gap value of the semiconductor catalytic material can be calculated. The E_g of the sample can be obtained by the relationship between $(\alpha hv)^2$ and hv, and the intersection of the tangent and the x-axis is the desired E_g [49].

The band gap values of CNH and Ag_3PO_4/CNH were calculated according to Eq. (2), as shown in Fig. 3b. It can be clearly seen that the band gap energy of pure CNH is 2.342 eV, as the mass ratio increases, the band gap energy of Ag_3PO_4/CNH with three different mass ratios decreases first and then increases. Among them, Ag_3PO_4/CNH (20 wt.%) has the narrowest band gap width, which is reduced from 2.342 to 2.309 eV, indicating that Ag_3PO_4/CNH (20 wt.%) had the strongest photocatalytic performance, and the results will be further verified by the following tests and subsequent MC-LR degradation experiments.

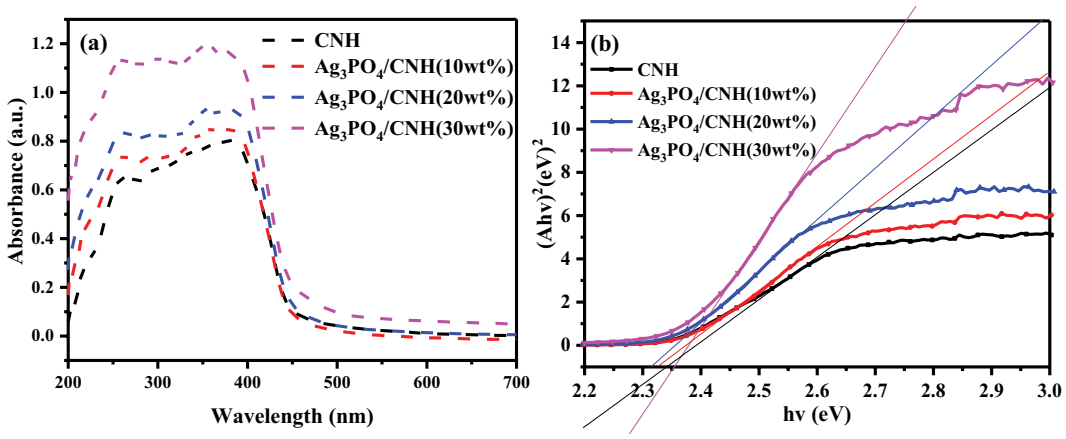

Fig. 3. (a) UV-Vis diffuse reflectance spectrometer of different samples and (b) corresponding band gap plots.

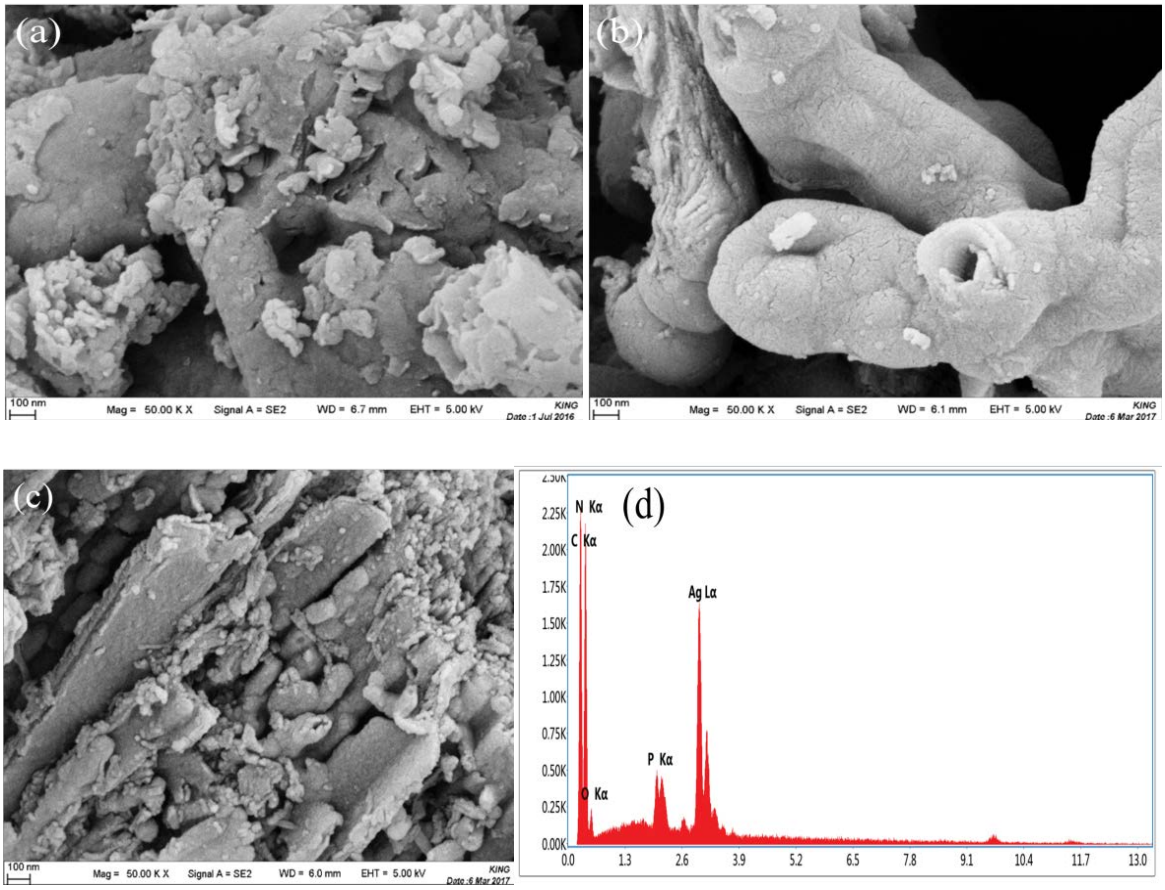

Fig. 4. SEM images of (a) g-C_3N_4, (b) CNH, (c) Ag_3PO_4/CNH (20 wt.%) and (d) EDS of Ag_3PO_4/CNH (20 wt.%).

3.1.4. SEM analysis

The scanning electron microscopy images of g-C_3N_4, CNH and Ag_3PO_4/CNH (20 wt.%) are shown in Fig. 4. It can be clearly seen that g-C_3N_4 is composed of many irregular nanosheets and has a typical graphite layered structure. This is consistent with that described in the literature [50] (Fig. 4a). Compared with g-C_3N_4, the particles agglomerated on the surface of CNH etched by HNO_3 are obviously smaller and some pores appear on the surface, indicating that the acid etching further increases the pores of the CNH catalyst (Fig. 4b). In addition, it can be clearly seen from Fig. 4c that Ag_3PO_4 is dispersed in the form of nanoparticles on the surface of CNH, the interaction between Ag_3PO_4 and CNH reduces the average size of Ag_3PO_4 nanoparticles and partly

prevented the agglomeration of Ag_3PO_4 particles, which is beneficial to improve the efficiency of photocatalytic reaction of composite materials [51,52], and the results will be further verified by subsequent MC-LR degradation experiments. The EDS spectra verified that the Ag_3PO_4/CNH composites were bound to contain C, N, O, P and Ag elements in Fig. 4d.

3.1.5. TEM analysis

To further explore the heterostructure of Ag_3PO_4/CNH composites transmission electron microscopy (TEM) test was performed for typical Ag_3PO_4/CNH (20 wt. %) as sample. As shown in Fig. 5a, the as-fabricated composite has sheet morphology and has some pores on the surface. There is direct contact between the CNH and nanoparticles of Ag_3PO_4 (50–100 nm) in the bulk heterojunction. The HRTEM image of Ag_3PO_4/CNH (20 wt.%) in Fig. 5b clearly shows the crystalline lattice fringes with the interplanar distance of 0.239 nm, which corresponds to the (211) plane of cubic Ag_3PO_4 phase [53]. These results further indicate that the Ag_3PO_4/CNH (20 wt.%) nanocomposite has been successfully prepared.

3.2. Dark adsorption performance

Before the photocatalytic experiment, the mixed solution was stirred in the dark for 1 h to reach the adsorption–desorption equilibrium. It can be seen from Fig. 6 that the adsorption effect of g-C_3N_4 after nitric acid etching was improved obviously. Moreover, after compounding no more than 20 wt.% of Ag_3PO_4, the adsorption effect was almost unchanged. When the mass ratio of Ag_3PO_4 was up to 30 wt.%, the adsorption rate had decreased.

3.3. Photocatalytic degradation of MC-LR

In order to investigate the photocatalytic activity of the prepared g-C_3N_4, pure CNH and different mass ratios of Ag_3PO_4/CNH photocatalyst, the degradation of MC-LR solution under visible light was studied. To eliminate the possibility of self-decomposition of MC-LR, a blank experiment without any catalyst was carried out under the same conditions. As illustrated in Fig. 7a, it reveals that the photolysis of MC-LR without any photocatalysis could be ignored, the g-C_3N_4 and pure CNH under visible light had weaker degradation ability to MC-LR, the maximum degradation rate after reaction for 120 min was only about 8.1% and 14.7%., the degradation performance could be significantly improved after compounding Ag_3PO_4, which was 9.85 times higher than that of g-C_3N_4 and 5.4 times higher than that of pure CNH. It might be attributed to the composite of Ag_3PO_4, which could shorten the width between valence band and conduction band of CNH (Fig. 3), increased its absorption of visible light, thereby enhanced the generation of electron–hole and accelerated redox reaction [54].

On the other hand, the compounding amount of Ag_3PO_4 had a greater influence on the photocatalytic activity of CNH. As the mass ratio of Ag_3PO_4 increased from 10% to 20 wt.%, the degradation performance of Ag_3PO_4/CNH (20 wt.%) on MC-LR increased, and the maximum time reached 79.8% when the reaction time was 120 min. Further increasing the Ag_3PO_4 content to 30 wt.% in the composite leads to a

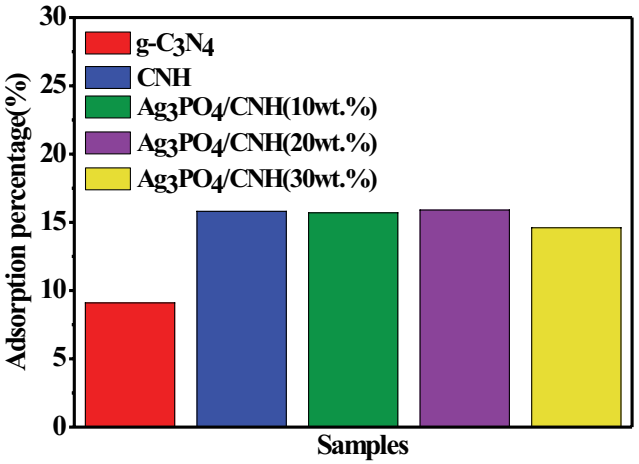

Fig. 6. Absorptive capacity of g-C_3N_4, pure CNH and heterojunction of Ag_3PO_4/CNH after reaching the adsorption equilibrium.

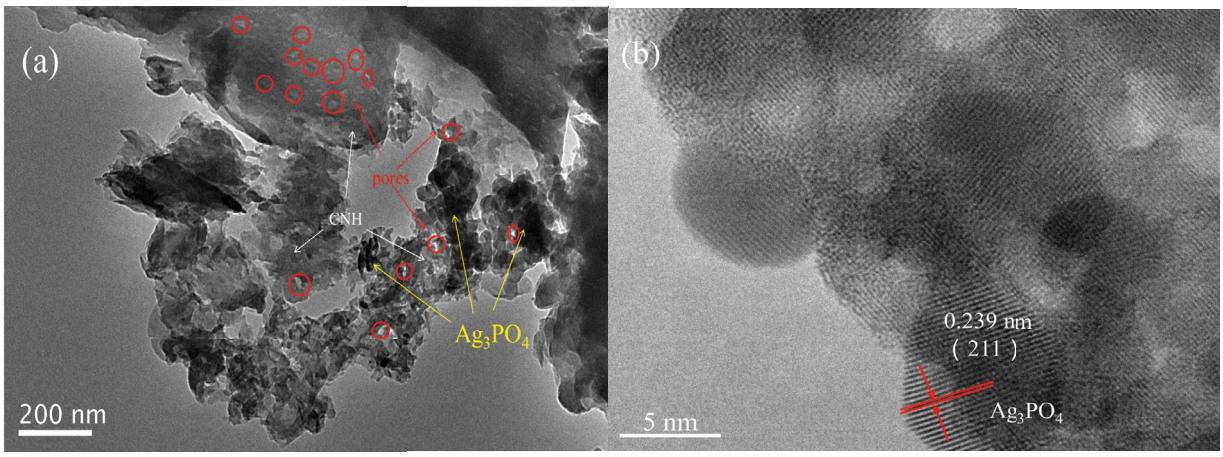

Fig. 5. (a) TEM image of Ag_3PO_4/CNH (20 wt.%) and (b) HRTEM image of Ag_3PO_4 on the Ag_3PO_4/CNH (20 wt.%).

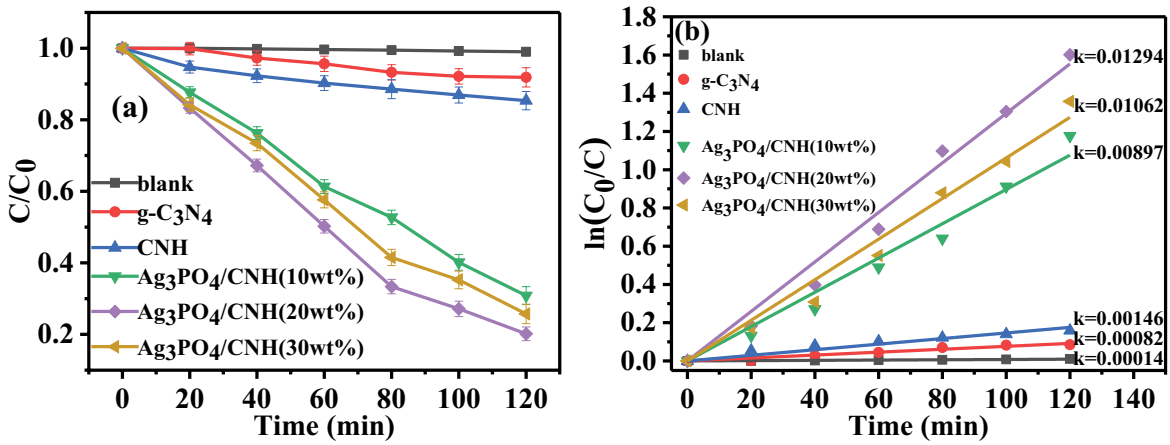

Fig. 7. Photodegradation of MC-LR with different photocatalyst Ag_3PO_4/CNH under visible-light: (a) analysis of performance and (b) kinetic analysis.

decreased photocatalytic activity. This was mainly because when the Ag_3PO_4 compounding amount was less than 20 wt.%, the active sites gradually increased with the increment of Ag_3PO_4, in this case, an effective charge separation can be achieved, resulting in improvement of photocatalytic activity and inhibition of photo-corrosion. At the same time, the band gap energy of Ag_3PO_4/CNH was less than that of pure CNH (Fig. 3b), and higher energy was still required to complete the catalytic reaction. Alternatively, when the Ag_3PO_4 compounding amount was more than 20 wt.%, it might be explained that the extra Ag_3PO_4 covered the CNH, which reduced the surface active sites on the CNH and was not conducive to carrier transfer. In this case, it reduced the amount of $^{\bullet}O_2^-$, h^+ or $^{\bullet}OH$ which might act as dominant reactive species in the photocatalytic degradation. At the same time, this can facilitate the recombination of photoinduced electron–hole pairs. Therefore, the photocatalytic activity will decrease with further increasing of the Ag_3PO_4 content [55].

In order to further quantify the photocatalytic activity of g-C_3N_4, pure CNH and three mass ratios of Ag_3PO_4/CNH, a first-order kinetic simulation was performed on the data of degradation of MC-LR under visible light, as shown in Eq. (3) [56] and the results are shown in Fig. 7b and Table 1. The results showed that the process of degradation of MC-LR by g-C_3N_4, pure CNH and three mass ratios of Ag_3PO_4/CNH accorded with the first-order kinetic model, the degradation rates of MC-LR by g-C_3N_4, CNH, Ag_3PO_4/CNH (10 wt.%), Ag_3PO_4/CNH (20 wt.%) and Ag_3PO_4/CNH (30 wt.%) were 0.00082, 0.00146, 0.00897, 0.01294 and 0.01062, respectively. The results further confirmed that Ag_3PO_4/CNH (20 wt.%) had the best photocatalytic performance, and the kinetic constant over Ag_3PO_4/CNH (20 wt.%) was 15.78 and 8.86 times of g-C_3N_4 and pure CNH.

$$\ln(C_0 / C) = kt \tag{3}$$

where k is the rate constant of MC-LR degradation, t is the photoreaction time, C is the concentration of MC-LR in the solution at time t and C_0 is the initial concentration of MC-LR.

Table 1
Kinetic constants (K) and the relative coefficient (R^2) values for photocatalytic MC-LR degradation

Sample	Kinetic constants (K)	Relative coefficient (R^2)
Blank	0.00004	0.9888
g-C_3N_4	0.00082	0.9917
CNH	0.00146	0.9895
Ag_3PO_4/CNH (10 wt.%)	0.00897	0.9951
Ag_3PO_4/CNH (20 wt.%)	0.01294	0.9972
Ag_3PO_4/CNH (30 wt.%)	0.01062	0.9963

The stability of the Ag_3PO_4/CNH (20 wt.%) was analyzed by performing five circulation photocatalytic reactions of the MC-LR samples. As shown in Fig. 8, the photodegradation efficiency was only reduced by 4.7% after five runs, indicating that the sample remained highly stable during the photocatalytic degradation of microcystins. A slight decrease in photocatalytic performance may be due to centrifugation and washing of the catalyst in the cycle experiment, and it may be also due to the photoetching during photocatalysis.

3.4. Discussion on photocatalytic mechanism analysis of Ag_3PO_4/CNH composites

Recombination and migration of electron–hole pairs of the support in photocatalysts are typically detected using photoluminescence (PL) spectroscopy. The PL intensity can reflect the recombination rate of electron–hole pairs in the catalysts. In order to better understand the mechanism of photocatalytic degradation of MC-LR, the two typical samples (CNH and Ag_3PO_4/CNH [20 wt. %]) were measured using PL. The fluorescence scanning range is 375–625 nm, the excitation wavelength is 300 nm, and the samples shows strong photoluminescence emission at about 440 nm, the results are shown in Fig. 9. It can be seen from the fluorescence spectrum that the PL emission intensity of Ag_3PO_4/CNH

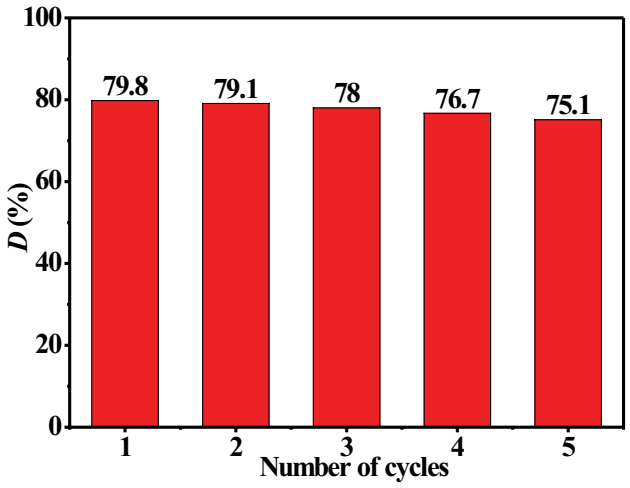

Fig. 8. Photocatalytic degradation of MC-LR under visible light over five circles with Ag_3PO_4/CNH (20 wt.%).

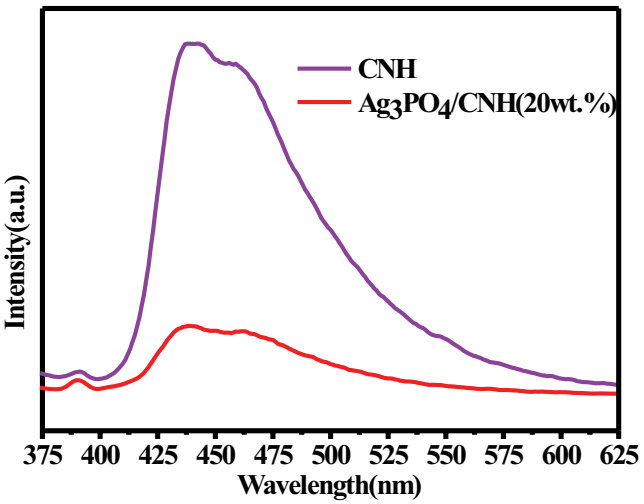

Fig. 9. Photoluminescence spectra of pure CNH and Ag_3PO_4/CNH (20 wt.%).

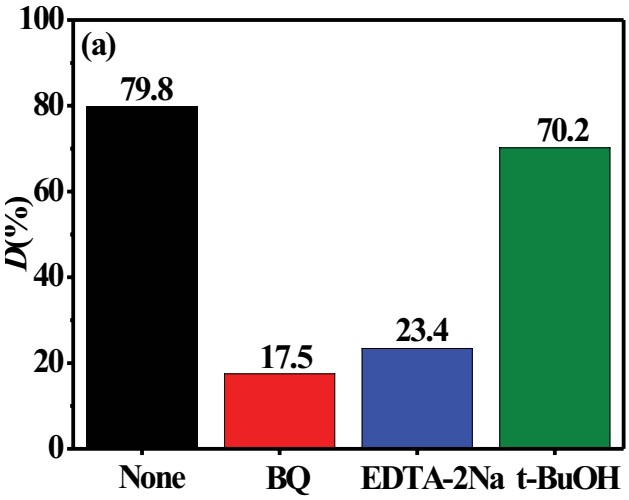

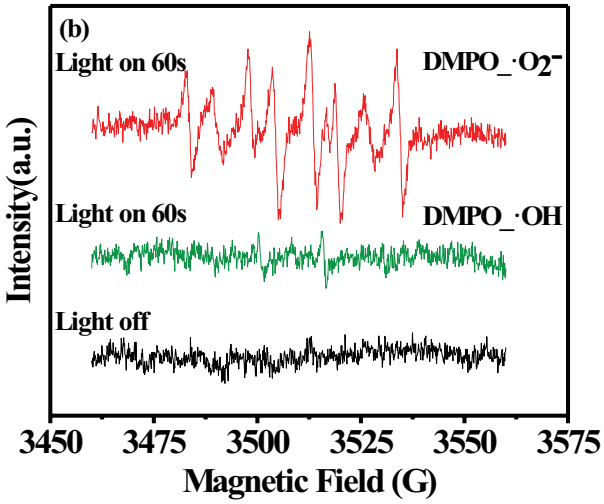

Fig. 10. (a) Comparison of photodegradation performance of MC-LR over Ag_3PO_4/CNH (20 wt.%) under the action of BQ, EDTA-2Na and t-BuOH scavenger and (b) ESR signals of $^{\bullet}O_2^-$ and $^{\bullet}OH$ in Ag_3PO_4/CNH (20 wt.%) under visible light.

(20 wt.%) is significantly lower than that of CNH, indicating that the recombination rate of photogenerated electrons and holes in the composite sample was relatively low. Therefore, composite samples have better photocatalytic performance.

To determine the main active species during the degradation with Ag_3PO_4/CNH (20 wt.%), quenching experiment was performed. Scavengers such as p-benzoquinone (BQ), ethylene diamine tetraacetic acid disodium salt (EDTA-2Na), and tertiary butanol (t-BuOH) are typically used to quench $^{\bullet}O_2^-$, h^+ and $^{\bullet}OH$, respectively [57]. As presented in Fig. 10a, the degradation efficiency of MC-LR was significantly limited after the addition of BQ or EDTA-2Na, indicating that $^{\bullet}O_2^-$ and h^+ had great impact on the photodegradation process. However, when t-BuOH was added, the degradation efficiency was only reduced by 9.6%. The change was not obvious compared with the addition of BQ and EDTA-2Na. The scavenger tests indicated that $^{\bullet}O_2^-$ and h^+ were the major active species, while $^{\bullet}OH$ was the minor one.

To further verify the above conclusions, ESR measurements were performed to detect radical species. As shown in Fig. 10b, after visible light irradiation of Ag_3PO_4/CNH (20 wt.%) for 60 s, the peak intensity of $^{\bullet}O_2^-$ was significantly stronger than $^{\bullet}OH$. This indicated that the amount of $^{\bullet}O_2^-$ was more than that of $^{\bullet}OH$, which proved that $^{\bullet}O_2^-$ was the main active species. The results were consistent with the scavenger tests.

Based on the above analysis, the mechanism diagram of degradation of MC-LR by Ag_3PO_4/CNH under visible light was plotted. As shown in Fig. 11, the band gap width of Ag_3PO_4 and CNH is 2.37 [58,59] and 2.342 eV (Fig. 3b), respectively. Both of them could be activated by the visible region, and photogenerated electrons were transferred from their VB to CB, so that photogenerated holes were produced at VB. Based on the existing research reports, the conduction bands (CB) of CNH and Ag_3PO_4 are −1.16 and +0.45 eV, respectively [60,61]. Therefore, according to the formula

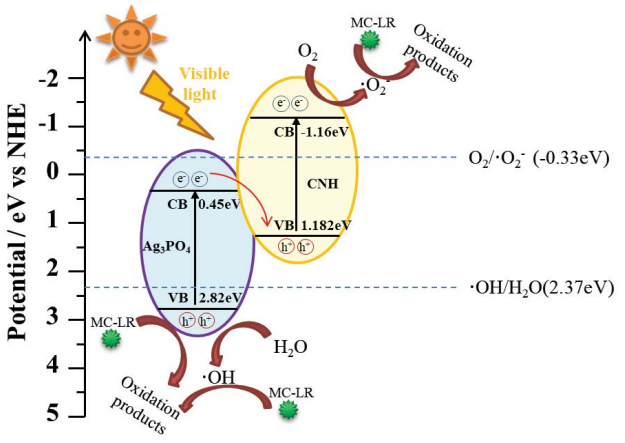

Fig. 11. Possible Z-scheme degradation mechanism.

$E_{CB} = E_{VB} - E_g$ [48], the valence bands (VB) of CNH and Ag_3PO_4 are 1.182 and 2.82 eV, respectively. However, $^{\bullet}O_2^-$ radicals could not be produced on the surface of Ag_3PO_4 because the CB potential (0.45 eV vs. NHE) was more positive than $O_2/^{\bullet}O_2^-$ (−0.33 eV vs. NHE) [60]. In addition, because the VB potential of CNH (1.182 eV vs. NHE) was more negative than $^{\bullet}OH/H_2O$ (+2.37 eV vs. NHE) [61], $^{\bullet}OH$ radicals could not be produced on the surface of CNH. Therefore, it was predicted that the heterojunction formed by the combination of Ag_3PO_4 and CNH could be explained by the Z-scheme degradation mechanism (Fig. 11). The VB potential of Ag_3PO_4 (2.82 eV vs. NHE) was more positive than $^{\bullet}OH/H_2O$ (+2.37 eV vs. NHE), so the photogenerated holes in the VB of Ag_3PO_4 could react with H_2O molecules to form $^{\bullet}OH$ or oxidize MC-LR directly. As for the electrons stored in the CB of CNH (−1.16 eV vs. NHE), the potential was more negative than $O_2/^{\bullet}O_2^-$(−0.33 eV vs. NHE), so the electrons could react with the dissolved O_2 to produce strong oxidizing $^{\bullet}O_2^-$, thereby degrading MC-LR. In addition, the CB of Ag_3PO_4 was closer to the VB of CNH than the CB of CNH. In this case, the photogenerated electrons on the CB of Ag_3PO_4 will be rapidly transferred to the VB of CNH. Therefore, in the Z- scheme degradation mechanism, the holes at the VB of CNH and the electrons transferred from the CB of Ag_3PO_4 will recombine [40], which greatly reduces the recombination rate of electrons and holes of Ag_3PO_4 and CNH itself, thereby increasing the photocatalytic activity.

4. Conclusion

The g-C_3N_4 prepared by the conventional polymerization method was subjected to hydrothermal acid etching of nitric acid to obtain the nanomaterial CNH. CNH has mesoporous characteristics and its photocatalytic performance is superior to that of pure g-C_3N_4. The Ag_3PO_4/CNH visible light catalyst was further successfully synthesized by chemical deposition method. Compared with CNH, the absorption of light was significantly enhanced and the absorption wave was red-shifted. The photocatalytic activity of Ag_3PO_4/CNH was the strongest when the mass ratio of Ag_3PO_4 was 20% in Ag_3PO_4/CNH composite, and the degradation rate of MC-LR was up to 79.8% within 120 min under visible light which was 9.85 times higher than that of g-C_3N_4 and 5.4 times higher than that of pure CNH. The degradation process accorded with quasi-first-order kinetic model and the kinetic constant of MC-LR degradation for Ag_3PO_4/CNH (20 wt. %) was 16.86 and 11.24 times of g-C_3N_4 and pure CNH. Furthermore, the scavenger tests proved that $^{\bullet}O_2^-$ and h^+ played the major role in the degradation process. A possible Z-scheme degradation mechanism of MC-LR over Ag_3PO_4/CNH hybrid was proposed based on the experimental results and band theory. In conclusion, the Ag_3PO_4/CNH (20wt.%) composite is a promising photocatalyst which can be recycled and has practical application value in water treatment engineering.

Acknowledgments

The authors are grateful for National Natural Science Foundation of China (No. 21477050), (No. 21607017), International Scientific and Technological Cooperation in Changzhou (CZ20140017).

References

[1] R. Xu, M.Y. Zhang, R.J.G. Mortimer, G. Pan, Enhanced Phosphorus Locking by Novel Lanthanum/Aluminum-Hydroxide Composite: implications for Eutrophication Control, Environ. Sci. Technol., 51 (2017) 3418–3425.
[2] Y.M. Liu, W. Chen, D.H. Li, Z.B. Huang, Y.W. Shen, Y.D. Liu, Cyanobacteria-/cyanotoxin-contaminations and eutrophication status before Wuxi Drinking Water Crisis in Lake Taihu, China, J. Environ. Sci., 23 (2011) 575–581.
[3] X.D. Duan, T. Sanan, D.L.C. Aa, X.X. He, M.H. Kong, D.D. Dionysiou, Susceptibility of the algal toxin microcystin-LR to UV/chlorine process: comparison with chlorination, Environ. Sci. Technol., 52 (2018) 8252–8262..
[4] J. Zhang, Q. Lu, Q. Ding, L. Yin, Y. Pu, A Novel and Native Microcystin-degrading bacterium of *Sphingopyxi* ssp. isolated from Lake Taihu, Int. J. Environ. Res. Public Health, 14 (2017) 1187.
[5] T. Fotiou, T.M. Triantis, T. Kaloudis, L.M. Pastrana-Martínez, V. Likodimos, P. Falaras, A.M.T. Silva, A. Hiskia, Photocatalytic degradation of microcystin-LR and off-odor compounds in water under UV-A and solar light with a nanostructured photocatalyst based on reduced graphene oxide–TiO_2 composite. Identification of intermediate products, Ind. Eng. Chem. Res., 52 (2013) 13991–14000.
[6] Q.Y. Sun, T.F. Zhang, F.F. Wang, C.Q. Liu, C.S. Wu, R.R. Xie, Y.Y. Zheng, Ultraviolet photosensitized transformation mechanism of microcystin-LR by natural organic matter in raw water, Chemosphere, 209 (2018) 96–103.
[7] J. Chang, Z.L Chen, Z. Wang, J.M. Shen, Q. Chen, J. Kang, L. Yang, X.W. Liu, C.X. Nie, Ozonation degradation of microcystin-LR in aqueous solution: intermediates, byproducts and pathways, Water Res., 63 (2014) 52–61.
[8] D.P. Ojha, J.H. Song, H.J. Kim, Facile synthesis of graphitic carbon-nitride supported antimony-doped tin oxide nanocomposite and its application for the adsorption of volatile organic compounds, J. Environ. Sci., 79 (2019) 35–42.
[9] A.C. Martins, A.L. Cazetta, O. Pezoti, J.R.B. Souza, T. Zhang, E.J. Pilau, T. Asefa, V.C. Almeida, Sol-gel synthesis of new TiO_2 /activated carbon photocatalyst and its application for degradation of tetracycline, Ceram. Int., 43 (2017) 4411–4418.
[10] Y.L. Su, Y.R. Deng, Y.X. Du, Alternative pathways for photocatalytic degradation of microcystin-LR revealed by TiO_2 nanotubes, J. Mol. Catal. A: Chem., 373 (2013) 18–24.
[11] W. Liu, M. Wang, C. Xu, S. Chen, X. Fu, Significantly enhanced visible-light photocatalytic activity of g-C_3N_4 via ZnO modification and the mechanism study, J. Mol. Catal. A: Chem., 368–369 (2013) 9–15.

[12] X. Yuan C. Zhou, Y. Jin, Facile synthesis of 3D porous thermally exfoliated g-C_3N_4 nanosheet with enhanced photocatalytic degradation of organic dye, J. Colloid Interface Sci., 468 (2016) 211–219.
[13] Z. Tong, Y. Dong, T. Xiao, T. Yao, Z. Jiang, Biomimetic fabrication of g-C_3N_4/TiO_2 nanosheets with enhanced photocatalytic activity toward organic pollutant degradation, Chem. Eng. J., 260 (2015) 117–125.
[14] J. Wang, F.Y. Su, W.D. Zhang, Preparation and enhanced visible light photoelectrochemical activity of g-C_3N_4/ZnO nanotube arrays, J. Solid State Electrochem., 18 (2014) 2921–2929.
[15] V.G. Deonikar, K.K. Reddy, W.J. Chung, H. Kim, Facile synthesis of Ag_3PO_4/g-C_3N_4 composites in various solvent systems with tuned morphologies and their efficient photocatalytic activity for multi-dye degradation, J. Photochem. Photobiol., A, 368 (2019) 168–181.
[16] Y. Hong, Y.Z. Hong, C.S. Li, B.X. Yin, D. Li, Z.Y. Zhang, B.D. Mao, W.Q. Fan, W. Gu, W.D. Shi, Promoting visible-light-induced photocatalytic degradation of tetracycline by an efficient and stable beta-Bi_2O_3@g-C_3N_4 core/shell nanocomposite, Chem. Eng. J., 338 (2018) 137–146.
[17] Y.Z. Hong, E.L. Liu, J.Y. Shi, X. Lin, L.Z. Sheng, M. Zhang, L.Y. Wang, J.H. Chen, A direct one-step synthesis of ultrathin g-C_3N_4 nanosheets from thiourea for boosting solar photocatalytic H_2 evolution, Int. J. Hydrogen Energy, 44 (2019) 7194–7204.
[18] L. Luo, W. Tang, C.J. Barrow, W. Yang, H. Wang, F. Jiang, Photocatalytic degradation of bisphenol A by HMS/g-C_3N_4 composite. Desal. Wat. Treat., 57 (2016) 1–8.
[19] J. Shen, H. Yang, Q. Shen, Y. Feng, Q. Cai, Template-free preparation and properties of mesoporous g-C_3N_4/TiO_2 nanocomposite photocatalyst, Crystengcomm, 16 (2014) 1868–1872.
[20] F. Tian, R. Zhu, F. Ouyang, Synergistic photocatalytic degradation of pyridine using precious metal supported TiO_2 with $KBrO_3$, J. Environ. Sci., 25 (2013) 2299–2305.
[21] X.M. Dang, X.F. Zhang, Y.T. Chen, X.L. Dong, G.W. Wang, C. Ma, X.X. Zhang. H.C. Ma, M. Xue, Preparation of β-Bi_2O_3/g-C_3N_4 nanosheet p–n junction for enhanced photocatalytic ability under visible light illumination, J. Nanopart. Res., 17 (2015) 1–8.
[22] H.J. Yan, H.X. Yang, TiO_2–g-C_3N_4 composite materials for photocatalytic H_2 evolution under visible light irradiation, J. Alloys Compd., 509 (2011) L26–L29.
[23] N. Boonprakob, N. Wetchakun, S. Phanichphant, D. Waxler, P. Sherrell, A. Nattestad, J. Chen, B. Inceesungvorn, Enhanced visible-light photocatalytic activity of g-C_3N_4/TiO_2 films, J. Colloid Interface Sci., 417 (2014) 402–409.
[24] W.K. Jo, N.C.S. Selvam, Z-scheme CdS/g-C_3N_4 composites with RGO as an electron mediator for efficient photocatalytic H_2 production and pollutant degradation, Chem. Eng. J., 317 (2017) 913–924.
[25] D. Ma, J. Wu, M.C. Gao, Y.J. Xin, T.J. Ma, Y.Y. Sun, Fabrication of Z-scheme g-C_3N_4 /RGO/Bi_2WO_6 photocatalyst with enhanced visible-light photocatalytic activity, Chem. Eng. J., 290 (2016) 136–146.
[26] W.J. Ong, L.K. Putri, L.L. Tan, S.P. Chai, S.T. Yong, Heterostructured AgX/g-C_3N_4 (X = Cl and Br) nanocomposites via a sonication-assisted deposition-precipitation approach: Emerging role of halide ions in the synergistic photocatalytic reduction of carbon dioxide, Appl. Catal., B, 180 (2016) 530–543.
[27] H. Xu, H.Z. Zhao, Y.H. Song, W. Yan, Y.G. Xu, H.P. Li, L.Y. Huang, S. Yin, Y.P. Li, Q. Zhang, H.M. Li, g-C_3N_4/Ag_3PO_4 composites with synergistic effect for increased photocatalytic activity under the visible light irradiation, Mater. Sci. Semicond. Process., 39 (2015) 726–734.
[28] X.Q. Geng, S. Chen, X. Lv, W. Jiang, T.H. Wang, Synthesis of g-C_3N_4/Bi_5O_7I microspheres with enhanced photocatalytic activity under visible light, Appl. Surf. Sci., 462 (2018) 18–28.
[29] C.J. Song, M.S. Fan, W.D. Shi, W. Wang, High-performance for hydrogen evolution and pollutant degradation of reduced graphene oxide/two-phase g-C_3N_4 heterojunction photocatalysts, Environ. Sci. Pollut. Res., 378 (2018) 1–13.
[30] X. Lin, D. Xu, Y. Xi, R. Zhao, L.N. Zhao, M.S. Song, H.J. Zhai, G.B. Che, L.M. Chang, Construction of leaf-like g-C_3N_4/Ag/$BiVO_4$ nanoheterostructures with enhanced photocatalysis performance under visible-light irradiation, Colloids Surf., A, 513 (2017) 117–124.
[31] Z.G. Yi, J.H. Ye, N. Kikugawa, T. Kako, S.X. Ouyang, H. Stuart-Williams, H. Yang, J.Y. Cao, W.J. Luo. Z.S. Li, Y. Liu, R.L. Withers, An orthophosphate semiconductor with photooxidation properties under visible-light irradiation, Nat. Mater., 9 (2010) 559–564.
[32] P.F. Zhu, Y.J. Chen, M. Duan, Z.H. Ren, M. Hu, Construction and mechanism of a highly efficient and stable Z-scheme Ag_3PO_4/reduced graphene oxide/Bi_2MoO_6 visible-light photocatalyst, Catal. Sci. Technol., 8 (2018) 3818–3832.
[33] Y.K. Jo, I.Y. Kim, J.M. Lee, S. Nahm, J.W. Choi, S.J. Hwang, Surface-anchored CdS@Ag_3PO_4 nanocomposite with efficient visible light photocatalytic activity, Mater. Lett., 114 (2014) 152–155.
[34] Y.M. He, L.H. Zhang, B.T. Teng, M.H. Fan, New application of Z-scheme Ag_3PO_4/g-C_3N_4 composite in converting CO_2 to fuel, Environ. Sci. Technol., 49 (2015) 649–656.
[35] Z.K. Cui, M.M. Si, Z. Zhi, L.W. Mi, W.J. Fa, H.M. Jia, Preparation and characterization of Ag_3PO_4/BiOI composites with enhanced visible light driven photocatalytic performance, Catal. Commun., 42 (2013) 121–124.
[36] M. Pirhashemi, A. Habibi-Yangjeh, S. Rahim Pouran, Review on the criteria anticipated for the fabrication of highly efficient ZnO-based visible-light-driven photocatalysts, J. Ind. Eng. Chem., 62 (2018) 1–25.
[37] R. Guo, J. Wu, A. Xu, X. Huang, H. Zhua, R. Jiang, Y. Lin, F. Guo, $ZnWO_4$/Ag_3PO_4 composites with an enhanced photocatalytic activity and stability under visible light, RSC Adv., 6 (2016) 114818–114824.
[38] Y.J. Chen, P.F. Zhu, M. Duan, J. Li, Z.H. Ren, P.P. Wang, Fabrication of a magnetically separable and dual Z-scheme PANI/Ag_3PO_4/$NiFe_2O_4$ composite with enhanced visible-light photocatalytic activity for organic pollutant elimination, Appl. Surf. Sci., 486 (2019) 198–211.
[39] L. Chen, K.Y.H. Gin, Y.L. He, Effects of sulfate on microcystin production, photosynthesis, and oxidative stress in Microcystis aeruginosa, Environ. Sci. Pollut. Res., 23 (2016) 3586–3595.
[40] Q. Guo, H. Li, Q. Zhang, Y.L. Zhang, Fabrication, characterization and mechanism of a novel Z-scheme Ag_3PO_4/NG/Polyimide composite photocatalyst for microcystin-LR degradation, Appl. Catal., B, 229 (2018) 192–203.
[41] Y.P. Sun, K. He, Q.D. Yin, S. Echigo, G.X. Wu, Y.T. Guan, Determination of quorum-sensing signal substances in water and solid phases of activated sludge systems using liquid chromatography–mass spectrometry, J. Environ. Sci., 69 (2018) 85–94.
[42] S. L. Wang, L.L. Wang, W.H. Ma, D.M. Johnson, Y.F. Fang, M.K. Jia, Y.P. Huang, Moderate valence band of bismuth oxyhalides (BiOXs, X = Cl, Br, I) for the best photocatalytic degradation efficiency of MC-LR, Chem. Eng. J., 259 (2015) 410–416.
[43] X. Ma, Y. Lv, J. Xu, Y. Liu, R. Zhang, Y. Zhu, A strategy of enhancing the photoactivity of g-C_3N_4 via doping of nonmetal elements: a first-principles study, J. Phys. Chem., C, 116 (44) (2012) 23485–23493.
[44] Y.M. He, J. Cai, T.T. Li, Y. Wu, Y.M. Yi, M.F. Luo, L.H. Zhao, Synthesis, characterization, and activity evaluation of $DyVO_4$/g-C_3N_4 composites under visible-light irradiation, Ind. Eng. Chem. Res., 51 (2012) 14729–14737.
[45] H. Katsumata, T. Sakai, T. Suzuki, S. Kaneco, Highly efficient photocatalytic activity of g-C_3N_4/Ag_3PO_4 hybrid photocatalysts through Z-scheme photocatalytic mechanism under visible light, Ind. Eng. Chem. Res., 53 (2014) 8018–8025.
[46] H. Ji, F. Chang, X. Hu, Q. Wei, J. Shen, Photocatalytic degradation of 2,4,6-trichlorophenol over g-C_3N_4 under visible light irradiation, Chem. Eng. J., 218 (2013) 183–190.
[47] S. C. Yan, Z. S. Li, Z. G. Zou, Photodegradation performance of g-C3N4 fabricated by directly heating melamine, Langmuir, 25 (2019) 10397–10401.

[48] J. Mei, D.P. Zhang, N. Li, M.X. Zhang, X.Y. Gu, S.C. Miao, S.H. Cui, J. Yang, The synthesis of Ag_3PO_4/g-C_3N_4 nanocomposites and the application in the photocatalytic degradation of bisphenol A under visible light irradiation, J. Alloys Compd., 749 (2018) 715–723.
[49] M. R. Elahifard, S. Ahmadvand, A. Mirzanejad, Effects of Ni-doping on the photo-catalytic activity of TiO_2 anatase and rutile: simulation and experiment, Mater. Sci. Semicond. Process., 84 (2018) 10–16.
[50] S.F. Kang, Y. Fang, Y.K. Huang, L.F. Cui, Y.Z. Wang, H.F. Qin, Y.M. Zhang, X. Li, Y.G. Wang, Critical influence of g-C_3N_4 self-assembly coating on the photocatalytic activity and stability of Ag/AgCl microspheres under visible light, Appl. Catal., B, 168–169 (2015) 472–482.
[51] Y.P. Bi, S.X. Ouyang, J.Y. Cao, J.H. Ye, Facile synthesis of rhombic dodecahedral AgX/Ag_3PO_4 (X = Cl, Br, I) heterocrystals with enhanced photocatalytic properties and stabilities, Phys. Chem. Chem. Phys., 13 (2011) 10071–10075.
[52] H.Y. Huang, Y.Y. Feng, J.H. Zhou, G. Li, K.W. Dai, Visible light photocatalytic reduction of Cr(VI) on Ag_3PO_4 nanoparticles, Desal. Wat. Treat., 51 (2013) 7236–7240.
[53] J. Mei, D.P. Zhang, N. Li, M.X. Zhang, X.Y. Gu, S.C. Miao, S.H. Cui, J. Yang, The synthesis of Ag_3PO_4/g-C_3N_4 nanocomposites and the application in the photocatalyticdegradation of bisphenol A under visible light irradiation, J. Alloys Compd., 749 (2018) 715–723.
[54] H.T. Li, N. Li, M. Wang, B.P. Zhao, F. Long, Synthesis of novel and stable g-C_3N_4-Bi_2WO_6 hybrid nanocomposites and their enhanced photocatalytic activity under visible light irradiation, R. Soc. Open Sci., 5 (2018) 171419.
[55] L. Liu, Y.H. Qi, J.R. Lu, S.L. Lin, W.J. An, Y.H. Liang, W.Q. Cui, A stable Ag_3PO_4@g-C_3N_4 hybrid core@shell composite with enhanced visible light photocatalytic degradation, Appl. Catal., B, 183 (2016) 133–141.
[56] F.T. Li, Y. Zhao, Y. J. Hao, X.J. Wang, R.H. Liu, D.S. Zhao, D.M. Chen, N-doped P25 TiO_2-amorphous Al_2O_3 composites: one-step solution combustion preparation and enhanced visible-light photocatalytic activity, J. Hazard. Mater., 239–240 (2012) 118–127.
[57] F. Zhang, H. Peng, S.Q. Jiang, C.Q. Wang, X. Xu, L.P. Wang, Construction of precious metal-loaded BiOI semiconductor materials with improved photocatalytic activity for microcystin-LR degradation, Environ. Sci. Pollut. Res., 26 (2019) 8226–8236.
[58] P.F. Zhu, Y.J. Chen, M. Duan, M. Liu, P. Zou, Structure and properties of Ag_3PO_4/diatomite photocatalysts for the degradation of organic dyes under visible light irradiation, Powder Technol., 336 (2018) 230–239.
[59] Y.P. Liu, L. Fang, H.D. Lu, Y.W. Li, C.Z. Hu, H.G. Yu, One-pot pyridine-assisted synthesis of visible-light-driven photocatalyst Ag/Ag_3PO_4, Appl. Catal., B, 115–116 (2012) 245–252.
[60] Y. Huang, P.G. Wang, Z.Y. Wang, Y.F. Rao, J.J. Cao, S.Y. Pu, W.K. Ho, S.C. Lee, Protonated g-C_3N_4/Ti^{3+} self-doped TiO_2 nanocomposite films: Room-temperature preparation, hydrophilicity, and application for photocatalytic NO_x removal, Appl. Catal., B, 240 (2019) 122–131.
[61] M. Sun, Q. Zeng, X. Zhao, Y. Shao, P.G. Ji, C.Q. Wang, T. Yan, B. Du, Fabrication of novel g-C_3N_4 nanocrystals decorated Ag_3PO_4 hybrids: Enhanced charge separation and excellent visible-light driven photocatalytic activity, J. Hazard. Mater., 339 (2017) 9–21.